Research Article
Open Access
Life Sciences, Medicine and Biomedicine

Wound healing and anti-inflammatory activities of curcumin-loaded Pluronic® nanoformulation (NanoCUR) *in vitro*

Yih Wei Lim[1], Wan Shazlin Asmidar Wan Azhar[1], Seri Narti Edayu Sarchio[2] and Suhaili Shamsi[1*]

[1]*Laboratory of Animal Biochemistry and Biotechnology, Department of Biochemistry, Faculty of Biotechnology and Biomolecular Sciences, Universiti Putra Malaysia, 43400 Serdang, Selangor, Malaysia.*
[2]*Department of Biomedical Science, Faculty of Medicine and Health Sciences, Universiti Putra Malaysia, 43400 Serdang, Selangor, Malaysia.*

**Correspondence:* sh_suhaili@upm.edu.my

Received 7 October 2025; Revised 2 January 2026; Accepted 12 January 2026; Published online 18 March 2026

ABSTRACT

Wound healing is a complex biological process influenced by oxidative stress, inflammation, and cytokine activity. Current treatments are costly, inefficient, and often result in scarring. This study evaluates the wound healing potential of curcumin-loaded Pluronic® (PF) nanoformulation, NanoCUR, by assessing its antioxidant capacity, cytotoxicity, and effects on inflammatory cytokines *in vitro*. NanoCUR was synthesized by thin-film hydration method and was further characterized. The antioxidant capacity of NanoCUR was assessed using FRAP assay, while its cytotoxicity was evaluated in 3T3-NIH fibroblast cells. The wound healing property was determined through migration assay, and the IL-6 and TNF-α levels were monitored in LPS-induced RAW 264.7 macrophage cells by cytokine cytometry bead array (CBA). TNF-α expression was analyzed via Polymerase Chain Reaction (PCR). NanoCUR was successfully synthesized, producing nanoparticles with uniform morphology, high encapsulation efficiency (96.39%), and improved aqueous solubility. At 100 µM and 150 µM, NanoCUR exhibited enhanced antioxidant activity (6.78- and 3.89-% fold increment) compared to CUR respectively. Reduced toxicity of NanoCUR (20.63 µM) was observed in 3T3-NIH fibroblasts with higher LC_{50} values than CUR (14.16 µM) at 72h post treatment. NanoCUR enhanced fibroblast migration and wound closure by 1.45%, achieving complete wound closure at 5 µM within 72h, surpassing CUR. NanoCUR also demonstrated effective modulation of pro-inflammatory cytokines, reducing IL-6 and TNF-α levels, with suppression of TNF-α expression, supporting NanoCUR's anti-inflammatory mechanism at 5 µM and 10 µM. Collectively, the findings in the present study indicate that NanoCUR has improved antioxidant activity, biocompatibility, and cellular responses *in vitro*, which could serve as a fundamental basis to develop NanoCUR as a wound healing treatment.

Keywords: *Wound healing; NanoCUR; antioxidant; fibroblast migration; cytokine modulation and anti-inflammatory*

INTRODUCTION

Wound healing is a highly complex process, and an ideal wound dressing should fulfil several critical characteristics. These include maintaining moisture around the wound, being biocompatible, biodegradable, and non-toxic, stimulating growth factors, and providing protection against infections and microbial growth (Ghomi et al., 2019). Designing and developing suitable wound dressings for acute and chronic wounds remains a global challenge. Current therapeutic modalities, including hydrogels, hydrocolloids, alginate and skin substitutes are commonly utilized in the management of chronic wounds. However, a study involving 264 patients demonstrated that 77.6% of individuals receiving advanced treatment did not achieve wound healing within a three-month period (Morat & Ajemi., 2024). Moreover, the associated treatment costs range from RM5,000 to RM9,000 (Erni et al., 2023). These factors not only contribute to the high economic burden and extended healing times but also pose a risk of scarring, further complicating the management of chronic wounds.

https://doi.org/10.28916/lsmb.10.1.2026.231

Different drugs and delivery systems have been extensively investigated, targeting the aforesaid phases of wound healing. Yet, the presently available wound medication requires frequent applications, and wounds have increased risk of infections until the skin heals completely. Therefore, topical applications of compounds with antioxidative properties using proper materials and antioxidants will be useful against oxidative damage and to the healing of the wound. The current treatment options are expensive, limited, and inefficient, which lead to the development of new therapeutics to satisfy the unmet clinical needs.

The present study explores a plant-based compound as an alternative for wound healing. Herbal medicines and natural products have gained interest for their ability to accelerate and improve the healing process. They contain bioactive compounds with antibacterial and antifungal properties, while also exhibiting strong antioxidant effects that help reduce oxidative damage (Bowler et al., 2001; Khalifa et al., 2021). Additionally, these natural substances provide anti-inflammatory benefits, stimulate blood vessel formation, promote fibroblast growth, and aid in extracellular matrix synthesis, all of which are crucial for wound healing. Recent research continues to focus on enhancing the biological properties of wound healing agents, particularly curcumin (CUR) (Kumari et al., 2022).

CUR is a bioactive polyphenolic compound derived from the rhizomes of turmeric (Curcuma longa) and is recognized for its anti-inflammatory properties (Ghandadi & Sahebkar, 2016; Kocaadam & Sanlier, 2017; Mollazadeh et al., 2017). CUR inhibited the production of tumor necrosis factor alpha (TNF-α) (Jain et al., 2008), a key cytokine released from monocytes and macrophages that plays important roles in the regulation of inflammatory responses. It also functions as a scavenger of reactive oxygen species (ROS) during the inflammation phase, while enhancing granulation tissue formation and collagen deposition in the proliferation phase (Akbik et al., 2014). Recent studies have explored various CUR-based formulations to enhance wound healing efficacy, including hydrogels, nanofibrous scaffolds, and films (Deng et al., 2025). For instance, chitosan and sodium alginate–based hydrogel membranes loaded with CUR accelerated wound closure by ~75% within 14 days compared to gauze-covered wounds (Albarqi et al., 2022). Additionally, CUR-loaded carboxymethyl guar gum, reduced graphene oxide nanofibrous scaffolds demonstrated complete wound closure within 48h in 3T3 L1 fibroblast models (Orsu et al., 2021).

Despite these advantages, some limiting factors such as poor bioavailability (Shabnam et al., 2020; Stohs et al., 2020), low water solubility (Priyadarsini et al., 2014), and rapid metabolism (Yallapu et al., 2010; 2012) hinder the therapeutic efficacy of CUR. Moreover, CUR has been reported to exert cytotoxic effects. Specifically, exposure to 20 µM CUR reduced HaCAT cells viability by ~45% after 24h of treatment. In addition, when CUR-loaded wounds are exposed to light, CUR can act as a photosensitizer, triggering a pro-oxidant response that interferes with the transition from the inflammatory to proliferative phase of wound healing (Sharma et al., 2018). Scharstuhl et al. (2009) further demonstrated that high concentrations of CUR at 25 µM for 48h induced fibroblast apoptosis and impaired wound contraction via ROS-mediated pathways.

To overcome these limitations, the integration of nanoparticles (NPs) into wound care has emerged as a promising avenue. Among these approaches, polymeric micelles attracted interest for CUR delivery. Polymeric micelles are self-assembled nanoscale structures formed by amphiphilic block copolymers, consisting of a hydrophobic core and a hydrophilic shell (Negut & Bita, 2023). This architecture enhances solubilization of hydrophobic drugs, improves cellular uptake, and provides a protective environment that reduces drug degradation. Polymeric micelles exhibit favourable biocompatibility, stability under physiological conditions, and a lower risk of cytotoxicity, making them suitable carriers for wound healing applications (Negut & Bita, 2023; Wan et al., 2020). Among polymeric micellar systems, Pluronic®s® (PF) have been widely used as carrier and surfactants in pharmaceutical and biomedical applications. Pluronic®-F127 (PF127) is a triblock copolymer (poly(ethylene oxide)–poly(propylene oxide)–poly(ethylene oxide) (PEO–PPO–PEO) blocks, characterized by excellent biocompatibility and thermo-reversible gelation behaviour. PF127-based nanoformulations have been extensively explored for wound healing due to their ability to enhance drug residence time at the wound site, improve controlled drug release, and reduce local toxicity (Akbar et al., 2018; Almasian et al., 2021; Francisco et al., 2023; Li et al., 2023a; Zhang & Zhang, 2021).

The nanoformulation of CUR loaded into PF127 micelles (NanoCUR) exhibited promising stability (Shamsi, 2015), displayed an improved toxicity profile, and generated significantly lower reactive oxygen species (ROS) compared to CUR (Abdullah et al., 2022). However, the precise mechanisms through which NanoCUR can improve wound healing, mitigate oxidative stress, improving safety and efficacy, as well as modulating the level and expression of inflammatory cytokine compared to native CUR have not been fully explored. The present study sets to endeavour the feasibility of NanoCUR, a nanoformulation using Pluronic®-F127 (PF), an established pharmaceutical excipient in wound healing processes, specifically on the antioxidant properties and its effectiveness in promoting cell proliferation and mitigate inflammation.

MATERIALS AND METHODS

Materials

All reagents and solvents used were of the highest analytical grade. Distilled water was used throughout, unless otherwise stated. CUR, (≥ 98% purity), PF, phosphate-buffered saline (PBS), silver sulfadiazine (SSD), and sodium dodecyl sulphate (SDS) were obtained from Sigma Aldrich (Saint Louis, USA). Methanol (AR grade), chloroform (AR

grade), sodium acetate, iron (III) chloride hexahydrate ($FeCl_3 \cdot 6H_2O$), 2,4,6-tripyridyl-s-triazine (TPTZ), iron (II) sulphate heptahydrate, ascorbic acid, dimethyl sulfoxide (DMSO), and hydrochloric acid were procured from Fisher Scientific (Leicester, UK). Dulbecco's Modified Eagle's Medium (DMEM), penicillin-streptomycin, trypsin-EDTA, and thiazolyl blue tetrazolium bromide were purchased from Nacalai Tesque (Japan), while fetal bovine serum (FBS) was obtained from Tico Europe (Netherlands). The agarose gel used for electrophoresis was laboratory prepared. Molecular biology reagents included the innuPREP RNA Mini Kit 2.0 (IST Innuscreen GmbH, Berlin, Germany), Tetro cDNA Synthesis Kit (Meridian Bioscience, Bioline Reagent Ltd, UK), and the MyTaq Red Mix PCR Kit (Bioline Reagent Ltd, UK). All chemicals were handled and stored according to the manufacturer's instructions.

Preparation of CUR nanoformulation (NanoCUR)

Thin film hydration method adapted from Shamsi et al., (2015) was employed in the present study to prepare the NanoCUR. The particle hydrodynamic diameter, polydispersity index and zeta potential of NanoCUR were assessed by using Malvern Zetasizer Nano ZS instrument (Malvern Instruments, Malvern, UK). The surface functional groups of NanoCUR, CUR and PF were investigated with Fourier-Transform Infrared Spectroscopy (FTIR) technique using the Thermo Nicolet Model, Nicolet 6700 (Thermo Scientific, Waltham, MA, USA). The morphology of NanoCUR was observed using atomic force microscopy (AFM- Bruker Crest, Dimension Edge with Scanasyst). CUR content was quantified based on the absorbance value at 425 nm using spectrophotometer (Abdullah et al, 2022).

Antioxidant potential of NanoCUR by FRAP assay

0.5 mL of CUR and NanoCUR, prepared in methanol, and water, respectively at 100 µM and 150 µM, were mixed with 4.5 mL of FRAP reagent in a test tube. Solvent control was also included (100% methanol, and distilled water). The test tubes were then incubated at room temperature in a dark condition for 30 min. Absorbance of the samples was measured at 595 nm using spectrophotometer. In this assay, ascorbic acid at similar concentrations was used as the positive control. The concentrations chosen for both CUR and NanoCUR allow possible reliable comparison with positive control, the ascorbic acid. A standard solution of ferrous sulphate ($FeSO_4.7H_2O$) in increasing concentrations (0-800 µM) was prepared as calibration curve. The antioxidant potential was calculated based on the ability of a sample to reduce ferric ions and results were expressed as µmole Fe (II)/g fresh weight (FW) (Clarke et al., 2013).

Cell viability assay

3T3 murine fibroblast cell cultures (Passage 19) were obtained from American Type Culture Collection (ATCC) in a cryogenic form. 100 µL of cells suspension containing approximately 8 x 10^4 cells/mL was seeded onto 96-well plate and incubated in CO_2 incubator overnight until cells reached 80% confluency. Spent media was discarded and cells were washed once with 100 µL of pre-warmed PBS, pH 7.4. 200 µL of test samples was added into each well according to the plate design. The test samples include different concentrations of CUR (in 0.5% DMSO) and NanoCUR (dissolved in distilled water) at 0-100 µM. Cells were also exposed to the carrier, PF at 0-2% w/v, which were the concentrations of PF used to prepare NanoCUR, and 0.1% w/v of sodium dodecyl sulfate (SDS) as the positive control. Following samples exposure (24, 48 and 72h), cells were washed with pre-warmed PBS, pH 7.4 before they were incubated with 200 µL of fresh supplemented medium containing 20 µL of MTT reagent (0.5 mg/mL). After 4 h, the formazan crystals formed were solubilized with 100 µL of DMSO and quantified by absorbance measurement at 570 nm (Jenway, UK). The cell viability was calculated and reported as IC_{50} values (Seisenbaeva et al., 2021).

Migration assay

3T3 fibroblast cells (2 mL) were seeded onto 6-well plate (2.5 x10^4 cells/well) and incubated in CO_2 incubator until cells were grown into a confluent monolayer. The cells were then scratched with a sterile 200 µL pipette tip. Spent media was removed and cells were washed once with 1 mL of pre-warmed PBS, pH 7.4, followed by the addition of 2 mL of test samples: CUR (5 and 10 µM), NanoCUR (5, 10, 5 and 30 µM), and SSD (0.1% w/v) as the negative control. The concentrations for CUR and NanoCUR were selected based on cell viability experiment mentioned in the previous section. The scratch assay was performed in supplemented media containing only 1% FBS to minimize the possibility of cells proliferation and migration caused by the serum (Grada et al., 2017). Migration of the cells were evaluated under microscopic observation (Alexander et al., 2019). The images were captured using DinoLite microscope camera (Dino-Lite, USA) attached to the inverted microscope at 0, 12, 24, 48 and 72h of time interval post-treatment. The area of wound was quantified by using ImageJ imaging software (Version 2.14.0, MD, USA). The percentage of wound closure was calculated as follow:

$$Wound\ closure\ (\%) = \frac{Ao - At}{Ao} X\ 100\ \ (Equation\ 1)$$

Determination of pro-inflammatory cytokines level using Cytometric Beads Array (CBA) assay

RAW 264.7 macrophage cells were seeded with 1 mL of DMEM supplemented with 10% (v/v) FBS in a 24-well plate with a density of 5 x 10^4 cells per well. After 24h, the spent media in each well was removed. Then, phenol red-free DMEM supplemented with 2% (v/v) FBS and 1 µg/mL of LPS was added to each well and the cells were incubated for 2 h (Zailan et al., 2020). Following incubation, the cells were treated with CUR (5 and 10 µM) and NanoCUR (5, 10, 15 and 30 µM) for 24h. The concentrations chosen were based on the cell viability assay conducted on RAW 264.7 macrophage cells, prior to this experiment. The IC_{50} values for CUR and NanoCUR against RAW 264.7 macrophage cells were reported to be 12.73 ± 4.09 and 41.27 ± 4.44 µM, respectively.

All captured beads provided in the CBA mouse inflammation kit (BD Biosciences, USA) were vortexed and a master mix was prepared by adding 10 µL of each capture bead into the fluorescence-activated cell sorting (FACS) tube and vortexed. After 24h of incubation in the incubator, the samples were diluted with 1:50 dilution of assay diluent. Then, 50 µL of the master mix and 50 µL of the phycoerytherin (PE) detection reagent were added into each tube. The tubes were then incubated for 2 h in the dark at room temperature. After incubation, 1 mL of wash buffer was added into each tube, and the tubes were centrifuged at 200 x g for 5 min at 4°C. The supernatant was discarded slowly and 300 µL of wash buffer was added into the tube and centrifuged. Flow cytometry was performed by setting up the instrument using the Cytometer Setup Beads and samples were analysed for levels of IL-6 and TNF-α using the cytometer starting from the lowest concentration to the highest concentration of samples prepared. FCAP Array™ Software was used to generate and analyse the results accordingly.

Polymerase Chain Reaction (PCR)

The gene expressions of GAPDH, a housekeeping gene and TNF-α were assessed using a MyTaq Red Mix Kit (Bioline, London, UK). Each sample was analyzed in triplicates. Each reaction mixture had a total volume of 50 µL, comprising of 25 µL of MyTaq Red Mix, 4 ng/µL of cDNA, 1 µL of 20 µM forward primer, 1 µL of 20 µM reverse primer, and DEPC-treated water to adjust the final volume to 50 µL. The specific primer sequences for GAPDH and TNF-α are provided in Table 1 (Lee et al., 2012). The amplification protocol for PCR consisted of 30 cycles, starting with denaturation at 94°C for 45sec, followed by annealing at 63°C for TNF-α, and 64°C for GAPDH for 1min. This was followed by an extension step at 72°C for 45s. Gel electrophoresis of the PCR product (5 µL) was conducted on a 3.0% agarose gel at 100 V for 45 min in 1× TAE buffer (Vivantis Technologies, Kuala Lumpur Malaysia). The gel bands, visualized under UV light, were captured using the G:3Box gel doc (Syngene, Cambridge, UK). The intensity of the bands was measured using ImageJ (Version 2.14.0, MD, USA).

Table 1

Primer sequences of target genes for PCR analysis.

Target Gene	Gen Bank No.	Base Pair		Primer
GAPDH	M32599	269	Forward	5’-TGTTCCTACCCCCAATGTGT-3’
			Reverse	5’-CCCTGTTGCTGTAGCCGTAT-3’
TNF-α	NM_013693	324	Forward	5’-ACGGCATGGATCTCAAAGAC-3’
			Reverse	5’-CGGACTCCGCAAAGTCTAAG-3’

Note: The primer sequences used for gene expression analysis were adapted from Lee et al. (2012).

Statistical analysis

Statistical analyses were performed using One-Way Analysis of Variance (ANOVA), followed by Tukey’s post-hoc test for multiple comparisons, unless stated otherwise (GraphPad Prism 10, CA, USA). Statistical significance was denoted as follows: $p \leq 0.05$ (*), $p \leq 0.01$ (**), $p \leq 0.001$ (***), and $p \leq 0.0001$ (****). All experiments were conducted in triplicate, independently. Data are presented as mean ± standard deviation (SD).

RESULTS

Preparation and characterization of NanoCUR

The yellowish-orange colour of the lyophilized NanoCUR powder (Figure 1A) confirmed the successful encapsulation of CUR. NanoCUR exhibited improved solubility compared to native CUR, as demonstrated in aqueous dispersion studies (Figure 1B and 1C). Dynamic Light Scattering (DLS) analysis revealed that NanoCUR had an average size of 25.79

± 1.16 nm, and a polydispersity index (PDI) of 0.24 ± 0.01 indicating a monodispersed nanoparticle population with minimal aggregation. Zeta potential analysis showed a value of -2.11 ± 1.17 mV, attributed to the non-ionic nature of PF. Atomic Force Microscopy (AFM) demonstrated distinct differences between native CUR and NanoCUR. NanoCUR displayed a uniform spherical morphology with an average size range of 21.55 to 25.67 nm (Figure 2A), consistent with DLS measurements. As shown in Figure 2B, CUR exhibits strong peaks at 3460 cm^{-1} corresponding to hydroxyl groups, and at 1525 cm^{-1} due to C=C stretching. However, these peaks were absent in the NanoCUR spectra, suggesting that the aromatic structure of CUR may be partially shielded or altered upon encapsulation within the PF matrix. Additionally, peaks at 2905 cm^{-1} and 2885 cm^{-1} corresponding to aliphatic C-H stretching vibrations, were observed in both PF and CUR spectra, confirming the presence of both compounds in NanoCUR. Moreover, NanoCUR exhibited a peak at 1120 cm^{-1}, like PF, indicating the presence of both the hydrophilic PEO and the hydrophobic PPO core responsible for micellar formation. NanoCUR exhibited an average drug loading of 18.89 ± 0.59 mg CUR per g of NanoCUR and an encapsulation efficiency of 96.39 ± 3.04%.

Figure 1

The lyophilized NanoCUR powder and the aqueous solubility environment

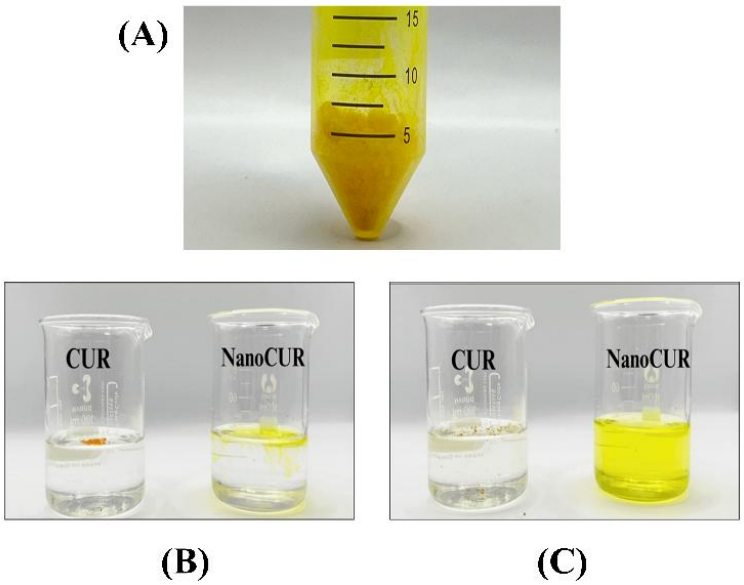

Note: (A) Figure shows the yellowish-orange flaky appearance of NanoCUR, indicating successful encapsulation and stabilization of CUR. (B) CUR exhibits poor solubility in water, leading to visible precipitation at the bottom of the beaker, whereas NanoCUR remains more evenly dispersed. (C) Further observation of the solubility behaviour shows that while CUR remains undissolved, NanoCUR achieves a more stable and uniform distribution in water.

Antioxidant potential of NanoCUR

Figure 3 shows the antioxidant potential of CUR and NanoCUR at varying concentrations (100 µM and 150 µM). As observed, NanoCUR demonstrated a significant improvement in antioxidant potential compared to CUR at both concentrations. At 100 µM, NanoCUR exhibited a statistically significant increase in antioxidant activity, and at 150 µM, the difference was even more pronounced.

Cytotoxicity of NanoCUR

Figure 4(A) illustrates CUR-induced cytotoxicity in 3T3-NIH fibroblast cells. Cell viability remained above 80% at concentrations ≤5 µM but declined significantly beyond 10 µM, with a time-dependent increase in toxicity. At concentrations of >30 µM, viability drastically decreased. In contrast, Figure 4(B) shows NanoCUR maintained viability >80% up to 10 µM, with a moderate decline at 15 µM. Even at >30 µM, NanoCUR-treated cells retained >30% viability, highlighting its protective effect. PF's biocompatibility is demonstrated in Figure 4(C), where cell viability remained >80% at concentrations of 0.1–0.5%. At 0.5% and 1%, viability initially decreased at 24 h but recovered by 72 h, indicating minimal long-term cytotoxicity. However, at >1%, a significant decline occurred, particularly at 48–72h. LC_{50} values (Table 2) further confirm NanoCUR's lower toxicity. At 24 h, LC_{50} for NanoCUR (91.87 ± 0.02 µM) was significantly higher than CUR (16.61 ± 0.01 µM), a consistent trend observed at 48 and 72h. PF exhibited low toxicity, with LC_{50} of 2.37 ± 0.01% w/v at 24h (Table 2). At 0.1–0.5%, cell viability remained high, while at >1%, cytotoxic effects became

more pronounced over time. Despite temporary reductions at 48 h, viability recovered at 72h, reinforcing PF's biocompatibility.

Figure 2

Morphology, particle size distribution and FTIR spectra

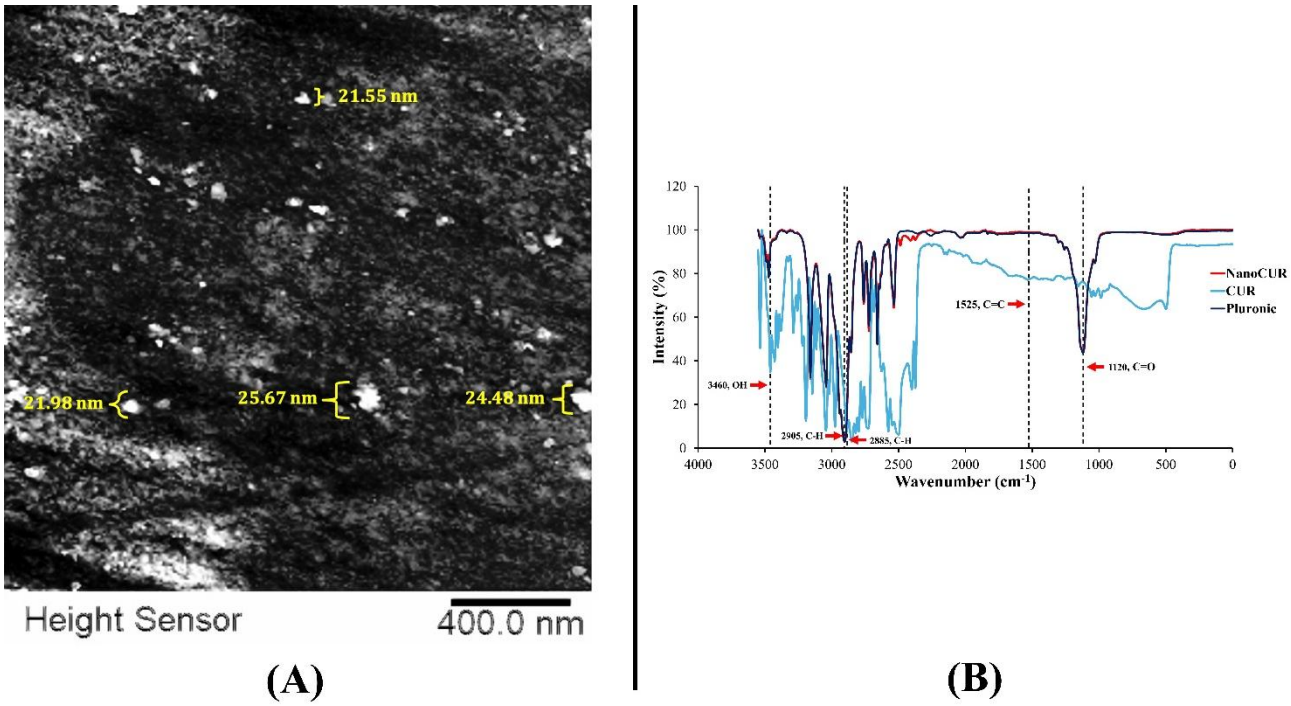

Note: (A) The image, captured using atomic force microscopy (AFM) at 1000× magnification, provides detailed insights into the morphology and size characteristics of the synthesized NanoCUR particles, illustrating their uniformity and size range. (B) The spectra show characteristic peaks representing functional groups such as the hydroxyl (O-H) stretching vibration at 3460 cm^{-1}, the aliphatic (C-H) stretching vibration at 2905 cm^{-1} and 2885 cm^{-1}, the alkene (C=C) stretching vibration at 1525 cm^{-1}, and the carbonyl (C=O) stretching vibration at 1120 cm^{-1}. Arrows in the figure highlight these specific characteristics peaks.

Figure 3

Antioxidant potential of CUR and NanoCUR at 100 and 150 µM

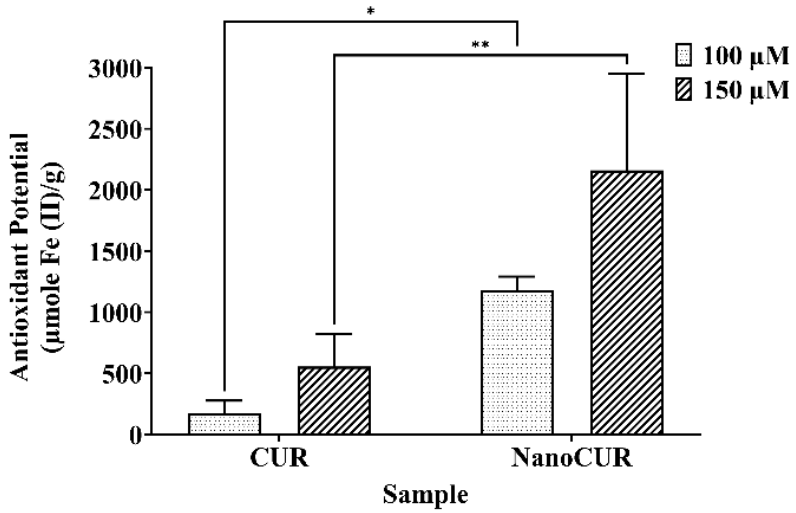

*Note: The significant difference analyzed using two-way ANOVA is indicated by the following thresholds, *p<0.05, **p<0.01.*

Figure 4

Cytotoxicity of CUR, NanoCUR, and Pluronic® (PF)

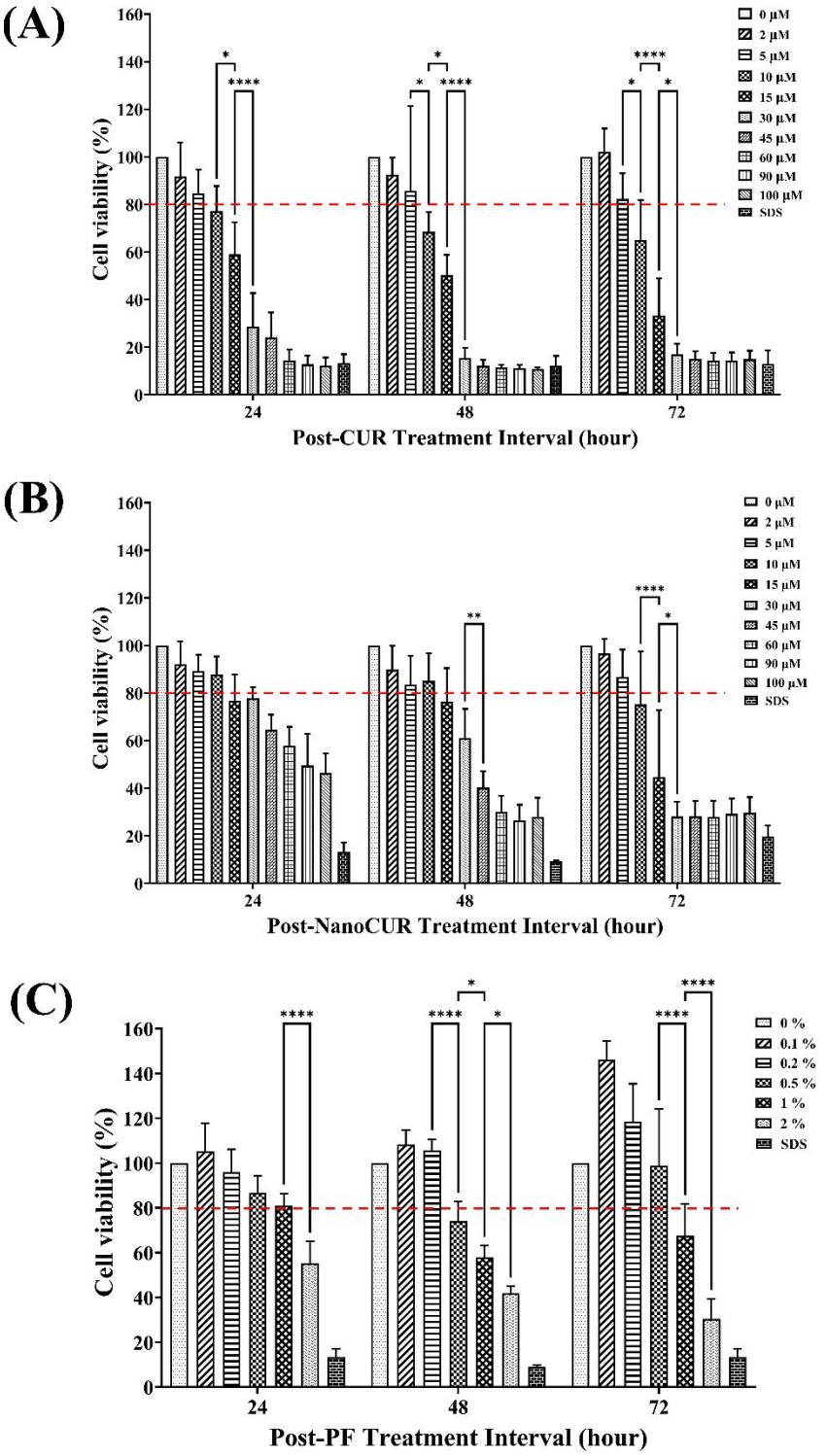

*Note: (A) CUR (2–100 µM), (B) NanoCUR (2–100 µM), and (C) Pluronic® (PF) (0.1%–2% w/v) against 3T3-NIH murine fibroblast cells over 24 to 72 hours. Significant differences analyzed using Two-Way ANOVA are indicated by the following thresholds: *p ≤ 0.05, **p ≤ 0.01, ****p ≤ 0.0001. The red dashed line represents 80% cell viability (ISO guideline, 2009).*

Table 2

IC_{50} values of CUR, NanoCUR, and PF following exposure against 3T3 cells over 24–72 h

Post-treatment (h)	IC_{50} (μM)		IC_{50} (% w/v)
	CUR	NanoCUR	PF
24	16.61 ± 0.01	91.87 ± 0.02[a]	2.37 ± 0.01
48	14.72 ± 0.02[b]	36.57 ± 0.05[ac]	1.38 ± 0.01[d]
72	14.16 ± 0.03[b]	20.63 ± 0.06[ac]	1.41 ± 0.01[d]

Note: Significance ($p < 0.05$): [a] indicates significant differences to CUR at respective time point, [b] to CUR, [c] to NanoCUR and [d] to PF between exposure time.

Migration assay

The untreated control group served as a baseline to observe the intrinsic migration capacity of cells in the absence of external treatments. Control shows no significant changes (Figure 5 and Figure 6) in wound closure across all time points, indicating that natural wound closure progresses at a steady, slow rate. The consistent performance of the control group establishes the reliability of the experimental design and provides a comparative framework for evaluating the effects of CUR and NanoCUR. The absence of active stimulation in the control group highlights the necessity of treatment to accelerate the wound-healing process. According to Figure 5 and 6, NanoCUR significantly enhanced migration compared to CUR, achieving complete wound closure at 5 μM by 72h, while CUR-treated cells showed residual gaps. The reduced migration at 10 μM CUR correlated with its cytotoxicity, whereas NanoCUR maintained viability and migration due to its lower cytotoxicity. The superior migration effect of NanoCUR aligns with its higher antioxidant potential. Conversely, 1% w/v PF did not promote wound closure and exhibited a slower migration rate than the control.

TNF-α and IL-6 levels

The reduction of TNF-α (Figure 7A) was measured in LPS-stimulated samples treated with different concentrations of CUR and NanoCUR. For TNF-α, both CUR and NanoCUR elicited concentration-dependent reductions across the tested range (2–30 μM). Notably, CUR at 15 μM produced a significantly greater TNF-α reduction (78.6 %) compared to NanoCUR (40.3%) ($p < 0.01$). At 30 μM, NanoCUR showed a decrease in TNF-α reduction (~45%), indicating a partial rebound in activity. No statistically significant differences were observed between CUR and NanoCUR at other concentrations.

For IL-6, both treatments significantly reduced cytokine production in a concentration-dependent manner, with maximum effects observed at 10 μM and 15 μM (Figure 7B). At 2 μM and 5 μM, both showed moderate reductions (~55–70%), with NanoCUR slightly more effective at 5 μM. At 10 μM and 15 μM, CUR reached its maximum IL-6 reduction (~100%), while NanoCUR was slightly less (~90%). Notably, NanoCUR continued to improve at 30 μM, showing IL-6 reduction of ~95%, suggesting a sustained dose-dependent anti-inflammatory effect. Collectively, these results indicate that CUR was superior to NanoCUT in TNF-α suppression at 15 μM, whereas both formulations exhibited comparable and robust IL-6 inhibitory effects at mid to high concentrations.

TNF-α Expression

Figure 8 shows that TNF-α expression was significantly reduced upon treatment with CUR and NanoCUR. At 5 μM, CUR significantly suppressed TNF-α expression compared to the negative control, demonstrating its anti-inflammatory potential. At 10 μM, CUR further reduced TNF-α expression, indicating a dose-dependent effect. This suppression is likely due to CUR's ability to inhibit the NF-κB pathway and its antioxidant activity. NanoCUR exhibited an even stronger effect at both concentrations, with a pronounced suppression of TNF-α.

DISCUSSION

Skins are exposed and not protected, making it susceptible to many injuries, including stabbed and burns. Physical injuries that cause tissue damage and disruption in the epithelial integrity of the skin and homeostasis are defined as wounds. Thus, skin loses its protective mechanism and provides pathway for the pathogens to invade human body that leads to significant morbidity and even death (Rosique et al., 2015). To counter injuries, wound healing processes will take place. Many cells, such as macrophages, neutrophils, platelets, and fibroblast cells are involved during the process

Figure 5

Migration assay of 3T3-NIH Murine fibroblast cells.

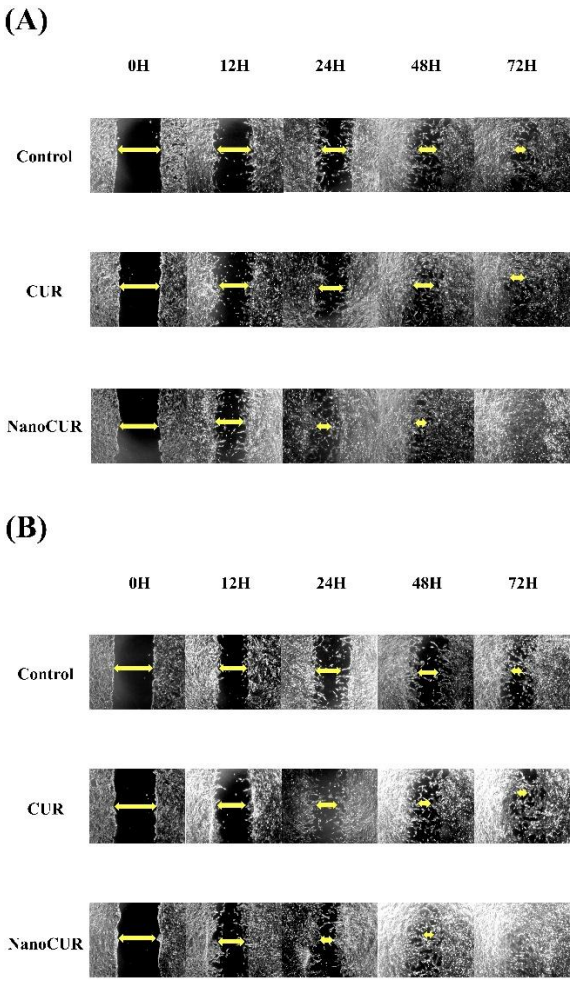

Note: Migration was assessed following exposure to control (media without treatment), CUR, and NanoCUR at (A) 5 µM and (B) 10 µM, observed at 0, 12, 24, 48, and 72 hours. Cells were grown in DMEM culture media supplemented with 1% FBS and observed under 10× magnification. The yellow double-headed arrows represent the distance of the wound area (cell-free area).

Figure 6

Wound progression of CUR and NanoCUR.

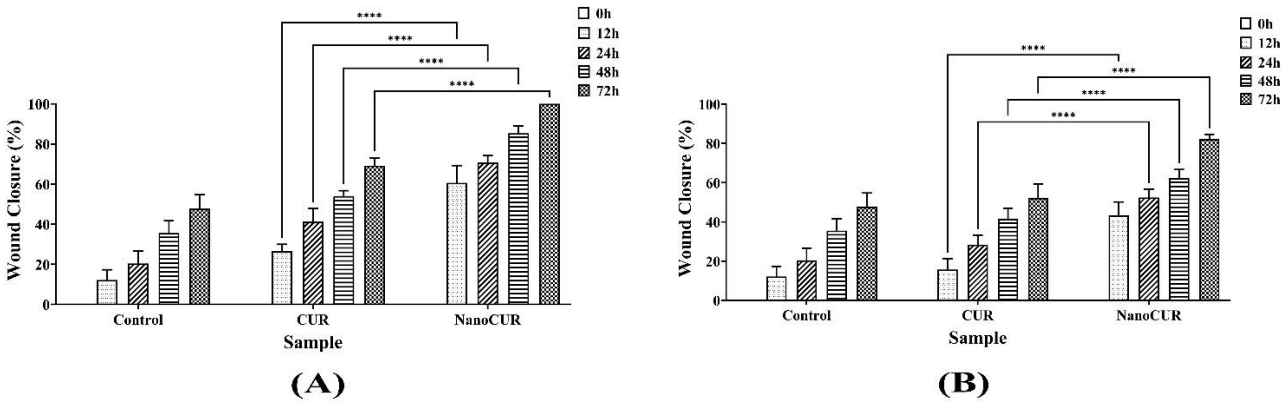

Note: Wound closure bar graph for samples at (A) 5 µM and (B) 10 µM. Media without treatment served as the control. Differences were analyzed using Two-Way ANOVA, followed by post-hoc Tukey's test. (****) indicates statistically significant differences ($p < 0.0001$) between the experimental groups.

Figure 7

Comparative effects of CUR and NanoCUR on LPS-induced TNF-α and IL-6 production

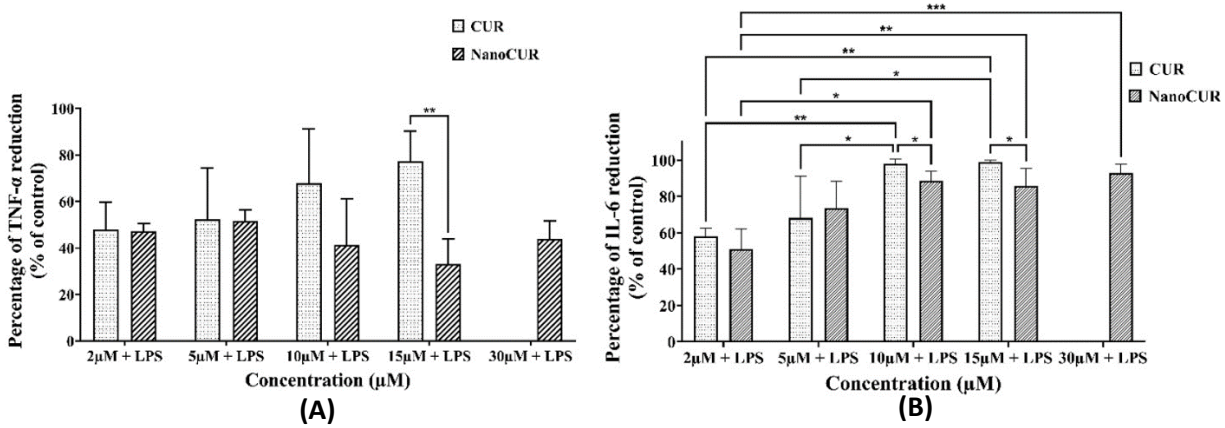

*Note: (A) Percentage reduction of TNF-α levels relative to LPS-stimulated control following treatment with CUR or NanoCUR (2–30 μM). CUR at 15 μM significantly reduced TNF-α compared to NanoCUR (**p < 0.01). (B) Percentage reduction of IL-6 levels relative to LPS-stimulated control. Both CUR and NanoCUR exhibited concentration-dependent suppression, with significantly greater reductions at 10 μM and 15 μM compared to lower concentrations (*p < 0.05, **p < 0.01 and ***p < 0.001). Data are presented as mean ± SD (n ≥3). Statistical significance was determined by One-way ANOVA followed by Tukey's post hoc test.*

Figure 8

Gene expression of TNF-α in response to CUR and NanoCUR treatments.

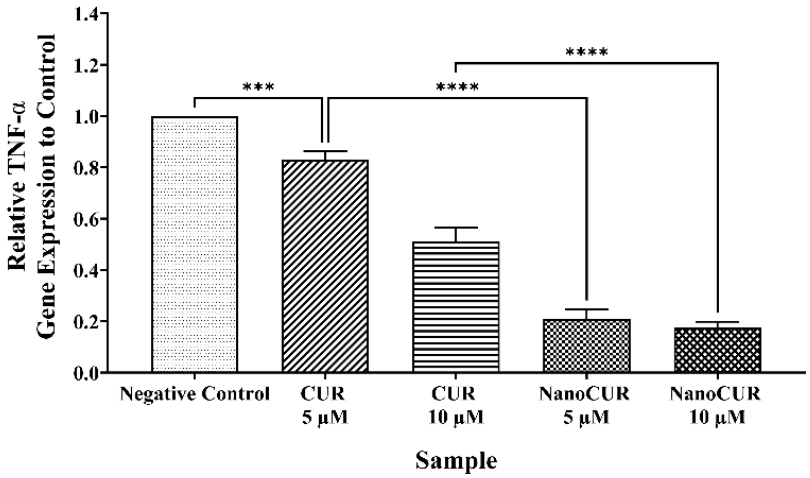

*Note: The graph shows the relative expression levels of TNF-α compared to the control in cells treated with CUR (5 μM and 10 μM) and NanoCUR (5 μM and 10 μM). NanoCUR demonstrated a more pronounced suppression of TNF-α at both concentrations (p<0.0001). Significant differences analyzed using One-Way ANOVA are indicated by the following thresholds: ***p ≤ 0.001, ****p ≤ 0.0001.*

of wound healing (Sinno & Prakash, 2013).During injury, fibroblast cells respond to migratory stimulus that are released then migrate to specific places, while at the same time releasing glycoprotein attractant so that other fibroblasts will be stimulated to follow the trails (Roussos et al., 2011).While wounded, cells that are involved and responsible for preventing pathogen from getting inside the body are neutrophils and macrophages that will engulf pathogen by phagocytosis in inflammation phase (auf Dem Keller et al., 2006; Nguyen et al., 2017).

In the migration assay, NanoCUR-treated cells closed nearly the entire wound, whereas CUR-treated cells showed a significantly slower migration rate with visible gaps persisting. This observation underscores NanoCUR's efficacy even at lower doses, which may reduce the risk of adverse effects. The slower migration observed with CUR at 10 μM likely reflects its dose-dependent toxicity. As shown in Figure 4(A), CUR exhibited dose-dependent toxicity, with significant reductions in cell viability at 10 μM, particularly at 48 and 72h. This cytotoxic effect limits the number of viable cells available for migration, thereby impairing wound closure. In contrast, NanoCUR demonstrated a more favourable

toxicity profile, with higher LC_{50} values compared to CUR (Table 2), allowing cells to maintain viability and sustain migration even at higher concentrations. The observed differences in migration rates between CUR and NanoCUR correlate strongly with their respective antioxidant potentials. As shown in Figure 3, NanoCUR exhibited significantly higher antioxidant activity than CUR. Antioxidants are critical in wound healing, as they mitigate oxidative stress, which can impair cellular function, inhibit migration, and delay tissue repair (Zhou et al., 2021). At wound sites, elevated ROS levels can cause oxidative damage, negatively impacting cell proliferation and motility. By neutralizing ROS, NanoCUR likely creates a more favourable cellular microenvironment for migration and repair. These findings are consistent with the work of Ma et al. (2024), which reported that antioxidants enhance cellular repair mechanisms and support wound healing by reducing oxidative stress.

Chronic inflammation is a key obstacle in wound healing, with prolonged inflammatory responses causing delays in tissue repair (Aswathanarayan et al., 2022) Elevated levels of pro-inflammatory cytokines, particularly tumor necrosis factor-alpha (TNF-α), contribute significantly to the disruption of the transition from the inflammatory phase to the proliferative phase (Nirenjen et al., 2023). TNF-α plays a critical role in immune regulation and inflammatory signalling, essential for defending against infection (Li et al., 2023b). However, its excessive production and persistence in wound healing conditions lead to chronic inflammation, which delays tissue repair and exacerbates wound conditions. Therefore, modulating TNF-α expression is crucial for promoting effective wound healing and facilitating the transition to the proliferative phase.

CUR and its nanoformulation, NanoCUR, have demonstrated strong anti-inflammatory effects (Yallapu et al., 2015), making them viable options for therapeutic wound-healing therapies. CUR targets a key regulator of inflammation, the NF-κB (Nuclear Factor kappa-light-chain-enhancer of activated B cells) pathway. IκB (Inhibitor of kappa B) proteins normally keep NF-κB dimers (p65/p50) dormant in the cytoplasm by blocking their translocation into the nucleus (Giridharan & Srinivasan, 2018). The IKK (IκB kinase) complex phosphorylates IκB in response to inflammatory stimuli, including infection, tissue damage, or the presence of pro-inflammatory cytokines including TNF-α and IL-1β. NF-κB dimers are released as a result of IκB breakdown (Karin & Ben-Neriah, 2000). The production of pro-inflammatory gene, such as TNF-α, is subsequently encouraged by these dimers' translocation to the nucleus, which prolongs inflammation and prevents wound healing (Karin & Ben-Neriah, 2000; Viatour et al., 2004).

CUR exerts its anti-inflammatory effects by interacting with multiple cellular pathways. A key mechanism involves its β-diketone structure, which contains two highly reactive carbonyl groups (C=O). These groups enable CUR to bind metal ions, such as zinc and copper, which are crucial for the activation of the NF-κB pathway. By binding to these metal ions, CUR inhibits the IKK complex, preventing the phosphorylation and degradation of IκB. As a result, NF-κB dimers remain sequestered in the cytoplasm, blocking the transcription of pro-inflammatory cytokines like TNF-α and IL-1β (Prasad et al., 2021; Smirnova et al., 2023; Yen et al., 2018). Moreover, CUR has antioxidant properties that contribute to its anti-inflammatory action. During inflammation, reactive oxygen species (ROS) are generated as a byproduct of immune cell activation. Excessive ROS can promote the activation of NF-κB, further exacerbating inflammation (Ranneh et al., 2017). CUR's ability to neutralize ROS directly reduces oxidative stress, preventing the activation of NF-κB and minimizing the associated inflammatory response (Huang et al., 2021). Furthermore, CUR interferes with upstream signalling pathways such as MAPK (mitogen-activated protein kinase) and TLR4-MD2 (Toll-like receptor 4-myeloid differentiation protein 2), which further suppress NF-κB activation, reinforcing its anti-inflammatory effects (Gradišar et al., 2007, Karthikeyan et al., 2020; Panaro et al., 2020).

The cytokine assays revealed a nuanced anti-inflammatory profile. While CUR outperformed NanoCUR in TNF-α suppression at certain higher concentrations (15 μM), NanoCUR maintained robust inhibition across a broader range and showed comparable IL-6 suppression. Notably, NanoCUR elicited a stronger downregulation of TNF-α gene expression at both tested concentrations, suggesting that improved cellular uptake and sustained intracellular delivery may potentiate transcriptional regulation. This aligns with the hypothesis that nanoformulation not only enhances pharmacokinetics but also modifies pharmacodynamics at the cellular level.

The findings of this study align with previous research emphasizing the advantages of nanoparticle formulations over their parent compounds. Zhuo et al. (2024) and Punfa et al. (2012) reported that nanoscale formulations improve solubility, stability, and cellular uptake, leading to enhanced therapeutic efficacy and reduced cytotoxicity. NanoCUR's superior migration-promoting effects, coupled with its antioxidant activity, support its potential as a multifunctional therapeutic agent for wound healing. The enhanced anti-inflammatory effect of NanoCUR aligns with its superior antioxidant capacity and better solubility. These properties contribute to NanoCUR's increased efficacy in reducing TNF-α expression, making it a more reliable therapeutic agent for modulating inflammation and promoting wound healing compared to traditional CUR.

CONCLUSION

The present study highlights the potential of NanoCUR, a curcumin-loaded Pluronic® (PF) nanoformulation, as a therapeutic agent for enhancing wound healing. This encapsulation also contributed to NanoCUR's superior antioxidant potential, as demonstrated in the FRAP assay, which showed significantly higher activity compared to CUR. These antioxidant properties are crucial for reducing oxidative stress during the wound healing process. Toxicity profiling

indicated that NanoCUR exhibited a significantly improved biocompatibility profile compared to CUR, with reduced cytotoxic effects observed at the tested concentrations. Furthermore, migration assays demonstrated that NanoCUR significantly enhanced wound closure rates, particularly at 5 µM concentration, outperforming CUR treatment over a 72-hour period. NanoCUR also effectively modulated inflammatory cytokine (TNF-α), reducing inflammation and supporting tissue regeneration. Collectively, the combination of improved solubility, antioxidant capacity, biocompatibility, and enhanced cellular interaction makes NanoCUR a promising candidate for wound healing applications.

AUTHOR CONTRIBUTIONS

Suhaili Shamsi was responsible for conceptualization of the study, contributed to the methodology, validation, formal analysis, investigation, provided resources, performed data curation, prepared the original draft, reviewing and editing the manuscript, supervised the project, managed project administration, and secured funding for the research. Yih Wei Lim and Wan Shazlin Asmidar Wan Azhar contributed to the methodology, validation, formal analysis and investigation. They were also involved in data curation and in the preparation of the original draft of the manuscript. Seri Narti Edayu Sarchio contributed to the review and editing of the manuscript and provided supervision for the study.

ETHICS APPROVAL

Not applicable.

FUNDING

This research was funded by Ministry of Higher Education, Malaysia under the Fundamental Grant Research Scheme (FRGS), grant number FRGS/1/2023/WAB04/UPM/02/21 and Universiti Putra Malaysia under the Geran Putra GP-IPS, grant number GP-IPS/2023/9742000.

CONFLICT OF INTEREST

The authors declare no conflicts of interest in this work.

REFERENCES

Abdullah, S. N. S., Subramaniam, K. A., Muhamad Zamani, Z. H., Sarchio, S. N. E., Md Yasin, F., & Shamsi, S. (2022). Biocompatibility study of curcumin-loaded Fluronic F127 nanoformulation (NanoCUR) against the embryonic development of zebrafish (*Danio rerio*). *Molecules*, *27*(14), 4493. https://doi.org/10.3390/molecules27144493

Akbar, M. U., Zia, K. M., Akash, M. S. H., Nazir, A., Zuber, M., & Ibrahim, M. (2018). In-vivo anti-diabetic and wound healing potential of chitosan/alginate/maltodextrin/Pluronic®-based mixed polymeric micelles: Curcumin therapeutic potential. *Int J Biol Macromol, 120* (Pt B), 2418-2430. https://doi.org/10.1016/j.ijbiomac.2018.09.010

Akbik, D., Ghadiri, M., Chrzanowski, W., & Rohanizadeh, R. (2014). Curcumin as a wound healing agent. *Life Sci*, *116*(1), 1–7. https://doi.org/10.1016/j.lfs.2014.08.016

Albarqi, H. A., Alqahtani, A. A., Ullah, I., Khan, N. R., Basit, H. M., Iftikhar, T., Wahab, A., Ali, M., & Badar, M. (2022). Microwave-assisted physically cross-linked chitosan-sodium alginate hydrogel membrane doped with curcumin as a novel wound healing platform. *AAPS PharmSciTech, 23*(2), 72. https://doi.org/10.1208/s12249-022-02222-y

Alexander, H., Syed, S.A., Yazan, L., Zakarial, F.A., & Ong, Y. (2019). Migration and proliferation effects of thymoquinone-loaded nanostructured lipid carrier (TQ-NLC) and thymoquinone (TQ) on in vitro wound healing models. *Evid-Based Compl Alt*, *2019(*1), 9725738. https://doi.org/10.1155/2019/9725738

Almasian, A., Najafi, F., Eftekhari, M., Shams Ardekani, M. R., Sharifzadeh, M., & Khanavi, M. (2021). Preparation of polyurethane/Pluronic® F127 nanofibers containing peppermint extract loaded gelatin nanoparticles for diabetic wounds healing: Characterization, in vitro, and in vivo studies. *Evid Based Complement Altern Med, 2021*, 6646702. https://doi.org/10.1155/2021/6646702

Aswathanarayan, J. B., Rao, P., Hm, S., Gs, S., & Rai, R. V. (2022). Biofilm-associated infections in chronic wounds and their management. *Adv Exp Med Biol*, 55–75. https://doi.org/10.1007/5584_2022_738

auf dem Keller, U., Kümin, A., Braun, S. & Werner, S. (2006) Reactive oxygen species and their detoxification in healing skin wounds. *J Invest Derm Symp P*, *11*(1):106-111. https://doi.org/10.1038/sj.jidsymp.5650001

Bowler, P. G., Duerden, B. I., & Armstrong, D. G. (2001). Wound microbiology and associated approaches to wound management. *Clin Microbiol Rev*, *14*(2), 244–269. https://doi.org/10.1128/CMR.14.2.244-269.2001

Clarke, G., Ting, K. N., Wiart, C., & Fry, J. (2013). High correlation of 2,2-diphenyl-1-picrylhydrazyl (DPPH) radical scavenging, Ferric reducing activity potential and total phenolics content indicates redundancy in use of all three assays to screen for antioxidant activity of extracts of plants from the Malaysian rainforest. *Antioxidants*, *2*(1), 1–10. https://doi.org/10.3390/antiox2010001

Deng, X., Ratnayake, J., & Ali, A. (2025). Curcumin-loaded drug delivery systems for acute and chronic wound management: A review. *Bioengineering (Basel), 12*(8), 860. https://doi.org/10.3390/bioengineering12080860

Erni, Z. R., Ku, N. K. A. R., & Izzuna, M. M. G. (2023). Negative pressure wound therapy. Ministry of Health Malaysia, Malaysian Health Technology Assessment Section (MaHTAS). https://www.moh.gov.my/en/publications-and-reports/policies-act-policies-guide-lines/penerbitan-klinikal/senarai-penerbitan-klinikal/senarai-laporan-kajian-teknologi-kesihatan-tr/negative-pressure-wound-therapy

Francisco, P., Neves Amaral, M., Neves, A., Ferreira-Gonçalves, T., Viana, A. S., Catarino, J., Faísca, P., Simões, S., Perdigão, J., Charmier, A. J., Gaspar, M. M., & Reis, C. P. (2023). Pluronic®® F127 hydrogel containing silver nanoparticles in skin burn regeneration: An experimental approach from fundamental to translational research. *Gels, 9*(3), 200. https://doi.org/10.3390/gels9030200

Ghandadi, M., & Sahebkar, A. (2016). Curcumin: An effective inhibitor of interleukin-6. *Curr Pharm Design*, *23*(6), 921–931. https://doi.org/10.2174/1381612822666161006151605

Ghomi, E. R., Khalili, S., Khorasani, S. N., Neisiany, R. E., & Ramakrishna, S. (2019). Wound dressings: Current advances and future directions. *J Appl Polym Sci*, 136(27), 47738. https://doi.org/10.1002/app.47738

Giridharan, S., & Srinivasan, M. (2018). Mechanisms of NF-κB p65 and strategies for therapeutic manipulation. *J Inflamm Res*, *11*, 407–419. https://doi.org/10.2147/JIR.S140188

Grada, A., Otero-Vinas, M., Prieto-Castrillo, F., Obagi, Z.& Falanga, V. (2017). Research techniques made simple: Analysis of collective cell migration using the wound healing assay. *J Invest Dermatol*, *137*(2), e11-e16. https://doi.org/10.1016/j.jid.2016.11.020

Gradišar, H., Keber, M. M., Pristovšek, P., & Jerala, R. (2007). MD-2 as the target of curcumin in the inhibition of response to LPS. *J Leukocyte Biol*, *82(*4), 968–974. https://doi.org/10.1189/jlb.1206727

Huang, J., Yi, Q., You, Y., Chen, Y., Niu, T., Li, Y., Zhang, J., Ji, X., Xu, G., Zou, W., Ji, F., & Luo, W. (2021). Curcumin suppresses oxidative stress via regulation of ROS/NF-κB signaling pathway to protect retinal vascular endothelial cell in diabetic retinopathy. *Mol Cell Toxicol*, *17*(3), 367–376. https://doi.org/10.21203/rs.3.rs-27239/v1

Jain, S. K., Rains, J., Croad, J., Larson, B., & Jones, K. (2008). Curcumin supplementation lowers TNF-A, IL-6, IL-8, and MCP-1 secretion in high glucose- treated cultured monocytes and blood levels of TNF-A, IL-6, MCP-1, glucose, and glycosylated hemoglobin in diabetic rats. *Antioxid Redox Sign*, *11*(2), 241–249. https://doi.org/10.1089/ars.2008.2140

Karin, M., & Ben-Neriah, Y. (2000). Phosphorylation meets ubiquitination: The control of NF-KB activity. *Annu Rev Immunol*, *18*(1), 621–663. https://doi.org/10.1146/annurev.immunol.18.1.621

Karthikeyan, A., Senthil, N., & Min, T. (2020). Nanocurcumin: A promising candidate for therapeutic applications. *Front Pharmacol*, *11*, 487. https://doi.org/10.3389/fphar.2020.00487

Khalifa, S. A. M., Shedid, E. S., Saied, E. M., Jassbi, A. R., Jamebozorgi, F. H., Rateb, M. E., Du, M., Abdel-Daim, M. M., Kai, G.-Y., Al-Hammady, M. A. M., Xiao, J., Guo, Z., & El-Seedi, H. R. (2021). Cyanobacteria—From the oceans to the potential biotechnological and biomedical applications. *Mar Drugs*, *19*(5), 241. https://doi.org/10.3390/md19050241

Kocaadam, B., & Şanlier, N. (2017). Curcumin, an active component of turmeric (*Curcuma longa*), and its effects on health. *Crit Rev Food Sci*, *57*(13), 2889–2895. https://doi.org/10.1080/10408398.2015.1077195

Kumari, A., Raina, N., Wahi, A., Goh, K. W., Sharma, P., Nagpal, R., Jain, A., Ming, L. C., & Gupta, M. (2022). Wound-healing effects of curcumin and its nanoformulations: A comprehensive review. *Pharmaceutics*, *14*(11), 2288. https://doi.org/10.3390/pharmaceutics14112288

Lee, K., Chow, Y., Sharmili, V., Abas, F., Alitheen, N. B. M., Shaari, K., Israf, D. A., Lajis, N. H., & Syahida, A. (2012). BDMC33, a curcumin derivative suppresses inflammatory responses in macrophage-like cellular system: Role of inhibition in NF-KB and MAPK signaling pathways. *Int J Mol Sci*, *13*(3), 2985–3008. https://doi.org/10.3390/ijms13032985

Li, S., Yang, C., Li, J., Zhang, C., Zhu, L., Song, Y., Guo, Y., Wang, R., Gan, D., Shi, J., Ma, P., Gao, F., & Su, H. (2023a). Progress in Pluronic® f127 derivatives for application in wound healing and repair. *Int J Nanomed, 18*, 4485-4505. https://doi.org/10.2147/IJN.S418534

Li, W., Liu, Q., Shi, J., Xu, X., & Xu, J. (2023b). The role of TNF-α in the fate regulation and functional reprogramming of mesenchymal stem cells in an inflammatory microenvironment. *Front Immunol*, *14*, 1074863. https://doi.org/10.3389/fimmu.2023.1074863

Ma, S., Ji, Z., Zhang, B., Geng, L., Cai, Y., Nie, C., Li, J., Zuo, Y., Sun, Y., Xu, G., Liu, B., Ai, J., Liu, F., Zhao, L., Zhang, J., Zhang, H., Sun, S., Huang, H., Zhang, Y., … Liu, G. (2024). Spatial transcriptomic landscape unveils immunoglobin-associated senescence as a hallmark of aging. *Cell*, *187*(24), 7025–7044.e34. https://doi.org/10.1016/j.cell.2024.10.019

Mollazadeh, H., Cicero, A. F. G., Blesso, C. N., Pirro, M., Majeed, M., & Sahebkar, A. Immune modulation by curcumin: The role of interleukin-10. *Crit Rev Food Sci*, *59*(1), 89–101. https://doi.org/10.1080/10408398.2017.1358139

Morat, N. S., & Ajemi, A. (2024). Prevalence and clinical characteristics of wound care patients in the northernmost state hospital of Malaysia: A retrospective analysis. *Wounds APAC*, *7*(2). https://woundsasia.com/wp-content/uploads/2024/12/WAPAC_7-2_6-9_morat-II.pdf

Negut, I., & Bita, B. (2023). Polymeric Micellar Systems—A Special Emphasis on "Smart" Drug Delivery. *Pharmaceutics*, *15*(3), 976. https://doi.org/10.3390/pharmaceutics15030976

Nguyen, V., Mendelsohn, A. & Larrick, J.W. (2017) Interleukin-7 and Immunosenescence. *J Immunol Res*, *2017*(1), 4807853. https://doi.org/10.1155/2017/4807853

Nirenjen, S., Narayanan, J., Tamilanban, T., Subramaniyan, V., Chitra, V., Fuloria, N. K., Wong, L. S., Ramachawolran, G., Sekar, M., Gupta, G., Fuloria, S., Chinni, S. V., & Selvaraj, S. (2023). Exploring the contribution of pro-inflammatory cytokines to impaired wound healing in diabetes. *Front Immunol*, *14*, 1216321. https://doi.org/10.3389/fimmu.2023.1216321

Orsu, P., Haider, H. Y., & Koyyada, A. (2021). Bioengineering for curcumin loaded carboxymethyl guargum/reduced graphene oxide nanocomposites for chronic wound healing applications. *In J Pharm*, 606, 120928. https://doi.org/10.1016/j.ijpharm.2021.120928

Panaro, M. A., Corrado, A., Benameur, T., Paolo, C. F., Cici, D., & Porro, C. (2020). The emerging role of curcumin in the modulation of TLR-4 signaling pathway: Focus on neuroprotective and anti-rheumatic properties. *Int J Mol Sci*, *21*(7), 2299. https://doi.org/10.3390/ijms21072299

Prasad, S., DuBourdieu, D., Srivastava, A., Kumar, P., & Lall, R. (2021). Metal–Curcumin complexes in therapeutics: An approach to enhance pharmacological effects of curcumin. *Int J Mol Sci*, *22*(13), 7094. https://doi.org/10.3390/ijms22137094

Priyadarsini, K. I. (2014). The chemistry of curcumin: From extraction to therapeutic agent. *Molecules, 19*(12), 20091–20112. https://doi.org/10.3390/molecules191220091

Punfa, W., Yodkeeree, S., Pitchakarn, P., Ampasavate, C., & Limtrakul, P. (2012). Enhancement of cellular uptake and cytotoxicity of curcumin-loaded PLGA nanoparticles by conjugation with anti-P-glycoprotein in drug resistance cancer cells. *Acta Pharmacol Sin*, *33*(6), 823–831. https://doi.org/10.1038/aps.2012.34

Ranneh, Y., Ali, F., Akim, A. M., Hamid, H. A., Khazaai, H., Fadel, A. (2017). Crosstalk between reactive oxygen species and pro-inflammatory markers in developing various chronic diseases: A review. *Appl Biol Chem*, *60*(3), 327–338. https://doi.org/10.1007/s13765-017-0285-9

Rosique, R.G., Rosique, M.J. & Farina Junior, J.A. (2015). Curbing inflammation in skin wound healing: A review. *Int J Inflamm*, 316235. https://doi.org/10.1155/2015/316235

Roussos, E.T., Condeelis, J.S. & Patsialou, A. (2011) Chemotaxis in cancer. *Nat Rev Cancer*, *11*(8), 573-587. https://doi.org/10.1038/nrc3078

Scharstuhl, A., Mutsaers, H. A. M., Pennings, S. W. C., Szarek, W. A., Russel, F. G. M., & Wagener, F. A. D. T. G. (2009). Curcumin-induced fibroblast apoptosis and in vitro wound contraction are regulated by antioxidants and heme oxygenase: Implications for scar formation. *J Cell Mol Med, 13*(4), 712-725. https://doi.org/10.1111/j.1582-4934.2008.00339.x

Seisenbaeva, G. A., Ali, L. M. A., Vardanyan, A., Gary-Bobo, M., Budnyak, T. M., Kessler, V. G., & Durand, J. O. (2021). Mesoporous silica adsorbents modified with amino polycarboxylate ligands–functional characteristics, health and environmental effects. *J Hazard Mater*, *406*, 124698. https://doi.org/10.1016/j.jhazmat.2020.124698

Shabnam, B., Harsha, C., Thakur, K. K., Khatoon, E., & Kunnumakkara, A. B. (2020). Curcumin: A potential molecule for the prevention and treatment of inflammatory diseases. *Royal Society of Chemistry*, 150–171. https://doi.org/10.1039/9781788015936-00150

Shamsi, S., Chen, Y.& Lim, L.Y. (2015). Characterization and biological properties of NanoCUR formulation and its effect on major human cytochrome P450 enzymes. *Int J Pharm, 495*, 194–203. https://doi.org/10.1016/j.ijpharm.2015.08.066

Shamsi. S, (2015). Development and evaluation of curcumin-loaded Pluronic® F127 nanoformulation Suhaili Shamsi. PhD Dissertation. University of Western Australia. https://research-repository.uwa.edu.au/en/publications/development-and-evaluation-of-curcumin-loaded-Pluronic®-f127-nanof/

Sharma, M., Sahu, K., Singh, S. P., & Jain, B. (2018). Wound healing activity of curcumin conjugated to hyaluronic acid: in vitro and in vivo evaluation. *Artif Cells Nanomed Biotechnol., 46*(5), 1009-1017. https://doi.org/10.1080/21691401.2017.1358731

Sinno, H. & Prakash, S. (2013). Complements and the wound healing cascade: An updated review. *Plast Surg Int*, 146764. https://doi.org/10.1155/2013/146764

Smirnova, E., Moniruzzaman, M., Chin, S., Sureshbabu, A., Karthikeyan, A., Do, K., & Min, T. (2023). A review of the role of curcumin in metal induced toxicity. *Antioxidants*, *12*(2), 243. https://doi.org/10.3390/antiox12020243

Stohs, S. J., Chen, O., Ray, S. D., Ji, J., Bucci, L. R., & Preuss, H. G. (2020). Highly bioavailable forms of curcumin and promising avenues for curcumin-based research and application: A review. *Molecules*, *25*(6), 1397. https://doi.org/10.3390/molecules25061397

Viatour, P., Merville, M., Bours, V., & Chariot, A. (2004). Protein phosphorylation as a key mechanism for the regulation of BCL-3 activity. *Cell Cycle*, *3*(12), 1498–1501. https://doi.org/10.4161/cc.3.12.1328

Wan, D., Li, C., & Pan, J. (2020). Polymeric micelles with reduction-responsive function for targeted cancer chemotherapy. *ACS Appl. Bio Mater., 3*(2), 1139-1146. https://doi.org/10.1021/acsabm.9b01070

Yallapu, M. M., Nagesh, P. K. B., Jaggi, M., & Chauhan, S. C. (2015). Therapeutic applications of curcumin nanoformulations. *AAPS J*, *17*(6), 1341–1356. https://doi.org/10.1208/s12248-015-9811-z

Yallapu, M.M., Gupta, B.K., Jaggi, M., & Chauhan, S.C. (2010). Fabrication of curcumin encapsulated PLGA nanoparticles for improved therapeutic effects in metastatic cancer cells. *J of Colloid Interf Sci*, *351*(1), 19-29. https://doi.org/10.1016/j.jcis.2010.05.022

Yallapu, M.M., Jaggi, M. & Chauhan, S.C. (2012) Curcumin nanoformulations: A future nanomedicine for cancer. *Drug Discov Today*, *17*(1-2), 71-80. https://doi.org/10.1016/j.drudis.2011.09.009

Yen, Y., Pu, C., Liu, C., Chen, Y., Chen, Y., Liang, C., Hsieh, J., Huang, H., & Chen, Y. (2018). Curcumin accelerates cutaneous wound healing via multiple biological actions: The involvement of TNF-α, MMP-9, α-SMA, and collagen. *Int Wound J*, *15*(4), 605–617. https://doi.org/10.1111/iwj.12904

Zailan, N. F. Z., Jaganathan, N., Sandramuti, T., Sarchio, S. N. E., & Hassan, M. (2020). Inhibition of GSK-3 by tideglusib suppresses activated macrophages and inflammatory responses in lipopolysaccharide-stimulated RAW 264.7 cell line. *Mal J Med Health Sci, 16*(SUPP9), 2-8. https://medic.upm.edu.my/upload/dokumen/2020110610495401_2020_0158.pdf

Zhang, Z., & Zhang, X. (2021). Curcumin loading on alginate nano-micelle for anti-infection and colonic wound healing. *J Biomed. Nanotechnol, 17*(6), 1160-1169. https://doi.org/10.1166/jbn.2021.3089

Zhou, X., Ruan, Q., Ye, Z., Chu, Z., Xi, M., Li, M., Hu, W., Guo, X., Yao, P., & Xie, W. (2021). Resveratrol accelerates wound healing by attenuating oxidative stress-induced impairment of cell proliferation and migration. *Burns*, *47*(1), 133-139. https://doi.org/10.1016/j.burns.2020.10.016

Zhuo, Y., Zhao, Y.G & Zhang, Y. (2024). Enhancing drug solubility, bioavailability, and targeted therapeutic applications through magnetic nanoparticles. *Molecules*, *29*(20), 4854. https://doi.org/10.3390/molecules29204854

Citation:

Lim, Y. W., Wan Azhar, W. S. A., Sarchio, S. N. E., & Shamsi, S. (2026). Wound healing and anti-inflammatory activities of curcumin-loaded Pluronic® nanoformulation (NanoCUR) *in vitro*. *Life Sciences, Medicine and Biomedicine*, *10*(1). https://doi.org/10.28916/lsmb.10.1.2026.231

Life Sciences, Medicine and Biomedicine
ISSN: 2600-7207